

UC San Diego

UC San Diego Previously Published Works

Title

Muscle wasting and adipose tissue browning in infantile nephropathic cystinosis

Permalink

<https://escholarship.org/uc/item/9z53z5vg>

Journal

Journal of Cachexia Sarcopenia and Muscle, 7(2)

ISSN

2190-5991

Authors

Cheung, Wai W
Cherqui, Stephanie
Ding, Wei
et al.

Publication Date

2016-05-01

DOI

10.1002/jcsm.12056

Peer reviewed

Muscle wasting and adipose tissue browning in infantile nephropathic cystinosis

Wai W. Cheung¹, Stephanie Cherqui¹, Wei Ding^{1,2}, Mary Esparza³, Ping Zhou^{1,4}, Jianhua Shao¹, Richard L. Lieber^{3,5} & Robert H. Mak^{1*}

¹Department of Pediatrics, University of California, San Diego, CA, USA; ²Division of Nephrology, The 5th People's Hospital of Shanghai, Fudan University, Shanghai, China;

³Department of Orthopedic Surgery, University of California, San Diego, CA, USA; ⁴Department of Pediatrics, The 2nd Hospital of Harbin Medical University, Harbin, China;

⁵Rehabilitation Institute of Chicago, Chicago

Abstract

Background Muscle wasting is a common complication in patients with infantile nephropathic cystinosis, but its mechanism and association with energy metabolism is not known. We define the metabolic phenotype in *Ctns*^{-/-} mice, an established murine model of infantile nephropathic cystinosis, with focus on muscle wasting and energy homeostasis.

Methods Male *Ctns*^{-/-} mice and wild-type (WT) controls were studied at 1, 4, 9, and 12 months of age. As *Ctns*^{-/-} mice started to develop chronic kidney disease (CKD) at 9 months of age, 9- and 12-month-old *Ctns*^{-/-} mice were also compared with age-matched WT mice with CKD. Serum and urine chemistry and energy homeostasis parameters were measured. Skeletal muscle histomorphometry and *in vivo* muscle function were measured. We studied expression of genes involved in muscle mass regulation, thermogenesis, energy metabolism, adipogenesis, and adipose tissue browning in *Ctns*^{-/-} mice.

Results *Ctns*^{-/-} mice showed loss of weight and lean mass and increased energy expenditure. *Ctns*^{-/-} mice exhibited abnormal energy homeostasis before the onset of their CKD. Food intake in *Ctns*^{-/-} mice was comparable with age-matched WT controls. However, significantly lower total body mass starting at 1 month of age and increased energy expenditure at 4 months of age preceded the onset of CKD at 9 months of age in *Ctns*^{-/-} mice. Muscle accept content in 1- and 4-month-old *Ctns*^{-/-} mice was significantly lower than that in age-matched WT controls. At 12 months of age, muscle fibre area and *in vivo* muscle strength was reduced in *Ctns*^{-/-} mice than that in WT or CKD controls. Muscle wasting in *Ctns*^{-/-} mice was associated with inhibition of myogenesis, activation of muscle proteolysis pathways, and overexpression of pro-inflammatory cytokines. Increased energy expenditure was associated with elevation of thermogenesis in skeletal muscle and adipose tissues. The development of beige adipocytes in *Ctns*^{-/-} mice is a novel finding. Expression of beige adipose cell surface markers (CD137, Tmem26, and Tbx1) and uncoupling protein-1, which is a brown adipose tissue marker, was observed in inguinal white adipose tissue of *Ctns*^{-/-} mice. Expression of key molecules implicated in the pathogenesis of adipose tissue browning (Cox2, cytochrome c oxidase subunit II; PGF2 α , prostaglandin F2 α ; IL-1 α , interleukin 1 α ; IL-6, interleukin 6; TNF- α , tumor necrosis factor α) was significantly increased in inguinal white adipose tissue of *Ctns*^{-/-} mice than that in WT controls.

Conclusion This study describes a mouse model of nephropathic cystinosis presenting with profound muscle wasting. The mechanism for hypermetabolism in *Ctns*^{-/-} mice may involve up-regulation of thermogenesis pathways in skeletal muscle and adipose tissues. This study demonstrates, for the first time, the development of beige adipocytes in *Ctns*^{-/-} mice. Understanding the underlying mechanisms of adipose tissue browning in cystinosis may lead to novel therapy.

Keywords Infantile nephropathic cystinosis; Adipocyte browning; Energy homeostasis; Muscle wasting; Cachexia

Received: 21 November 2014; Revised: 21 April 2015; Accepted: 3 June 2015

*Correspondence to: Robert H. Mak, Division of Pediatric Nephrology, University of California, San Diego, 9500 Gilman Drive, MC0630, La Jolla, CA 92093-0630, USA; Tel: 858 822 6717, Fax: 858 822 6776, Email: romak@ucsd.edu

Introduction

Cystinosis is a rare autosomal recessive disorder caused by mutations of the *CTNS* gene (17p13) encoding the lysosomal cystine transporter, cystinosin.¹ This results in the intralysosomal accumulation of cystine in all tissues, most notably the kidneys. Patients with infantile nephropathic cystinosis (INC) exhibit signs and symptoms of renal Fanconi syndrome and chronic kidney disease (CKD) in early childhood.² Muscle wasting is a common complication in patients with cystinosis. The prevalence of muscle weakness and myopathy varies from 33 to 60% in long-term follow-up studies of patients with INC.³⁻⁵ These complications negatively affect the quality of life due to decreased mobility and are associated with terminal events such as swallowing difficulty and respiratory musculature weakness leading to aspiration pneumonia, respiratory failure, and death.^{2,6} The underlying mechanism of muscle wasting in patients with INC is not well understood.^{2,7,8} In this study, we characterize the metabolic phenotype in *Ctns*^{-/-} mice, an established murine model of INC, with focus on muscle wasting and energy homeostasis.

Materials and methods

Mice

C57BL/6 *Ctns*^{-/-} mice were provided by Professor Corinne Antignac. Wild-type (WT) C57BL/6 control mice were acquired from Jackson Lab. Only male mice were used for this study. CKD was surgically induced in C57BL/6 mice by five-sixth nephrectomy.⁹ The study protocol was in compliance with Institutional Animal Care and Use Committee and National Institute of Health guidelines for the care and use of laboratory animals.

Serum and urine chemistry

Urine and serum phosphate, blood urea nitrogen (BUN), and bicarbonate levels were measured by standard laboratory methods (Table 1). Urine and serum creatinine levels were analysed using QuantiChrom creatinine assay kit (BioAssay Systems). Serum cystatin C levels were measured by enzyme-linked immunosorbent assay method (part number: ALX-850-328, Enzo Life Sciences). Protein levels in urine were measured using Pierce BCA protein assay kit. Tubular excretion of phosphorus (TEP) index was calculated according to the formula: $[\text{Phosphorus}_{\text{urine}} \div \text{Creatinine}_{\text{urine}}] \times [\text{Phosphorus}_{\text{serum}} \div \text{Creatinine}_{\text{urine}}] \times 100$.

Indirect calorimetry

Indirect calorimetry was performed in mice using Oxymax calorimetry (Columbus Instruments).⁹ Oxygen (VO₂) and carbon

Table 1 Urine and serum chemistry in mice during the course of the 12-month study

	WT control	<i>Ctns</i> ^{-/-}	WT control	<i>Ctns</i> ^{-/-}	WT control	<i>Ctns</i> ^{-/-}	WT control	<i>Ctns</i> ^{-/-}	WT control	<i>Ctns</i> ^{-/-}	WT control	<i>Ctns</i> ^{-/-}	CKD control	CKD control
	1 month	1 month	4 months	4 months	9 months	9 months	9 months	9 months	12 months	12 months	12 months	12 months	12 months	12 months
Urine chemistry														
Phosphate (μmol/24 h)	2.4 ± 0.5	3.5 ± 0.4	2.5 ± 0.3	4.1 ± 0.5 ^b	3.7 ± 0.5	4.7 ± 0.2 ^b	4.5 ± 0.2 ^b	4.5 ± 0.2 ^b	3.9 ± 0.2	6.5 ± 0.4 ^b	6.5 ± 0.4 ^b	5.9 ± 0.3 ^b	5.9 ± 0.3 ^b	5.9 ± 0.3 ^b
TEP (%)	12.2 ± 2.5	12.1 ± 2.1	10.6 ± 2.6	22.1 ± 5.4 ^b	17.8 ± 3.2	52.8 ± 6.7 ^b	43.7 ± 2.1 ^{b,c}	43.7 ± 2.1 ^{b,c}	16.4 ± 4.3	78.9 ± 12.3 ^b	78.9 ± 12.3 ^b	53.4 ± 2.3 ^{b,c}	53.4 ± 2.3 ^{b,c}	53.4 ± 2.3 ^{b,c}
Protein (mg/24 h)	6.7 ± 0.6	5.7 ± 0.3	8.4 ± 0.3	7.8 ± 0.5	10.8 ± 1.1	13.2 ± 0.6 ^b	12.5 ± 0.4 ^b	12.5 ± 0.4 ^b	13.8 ± 0.8	17.4 ± 1.1 ^b	17.4 ± 1.1 ^b	15.7 ± 0.2 ^b	15.7 ± 0.2 ^b	15.7 ± 0.2 ^b
Volume (mL/24 h)	0.4 ± 0.1	0.5 ± 0.2	0.6 ± 0.3	0.8 ± 0.4	0.8 ± 0.2	0.9 ± 0.3	0.8 ± 0.1	0.8 ± 0.1	0.6 ± 0.2	1.6 ± 0.2 ^b	1.6 ± 0.2 ^b	0.7 ± 0.3	0.7 ± 0.3	0.7 ± 0.3
Serum chemistry														
BUN (mg/dL)	32.9 ± 2.1	32.8 ± 1.4	32.7 ± 4.4	36.5 ± 2.2	35.6 ± 3.4	54.8 ± 3.4 ^b	45.7 ± 2.4 ^b	45.7 ± 2.4 ^b	31.7 ± 3.5	65.9 ± 4.7 ^b	65.9 ± 4.7 ^b	51.5 ± 2.3 ^{b,c}	51.5 ± 2.3 ^{b,c}	51.5 ± 2.3 ^{b,c}
Creatinine (mg/dL)	0.28 ± 0.04	0.23 ± 0.06	0.29 ± 0.07	0.29 ± 0.06	0.34 ± 0.05	0.43 ± 0.09	0.36 ± 0.11	0.36 ± 0.11	0.31 ± 0.03	0.52 ± 0.05 ^b	0.52 ± 0.05 ^b	0.42 ± 0.06 ^b	0.42 ± 0.06 ^b	0.42 ± 0.06 ^b
Creatinine clearance (μL/min)	65.4 ± 5.6	64.2 ± 9.5	58.9 ± 7.4	55.9 ± 6.3	67.8 ± 7.3	55.3 ± 6.7	59.8 ± 2.5	59.8 ± 2.5	72.3 ± 4.7	32.6 ± 3.6 ^a	32.6 ± 3.6 ^a	52.8 ± 2.6 ^{a,c}	52.8 ± 2.6 ^{a,c}	52.8 ± 2.6 ^{a,c}
Cystatin C (mg/dL)	0.08 ± 0.02	0.08 ± 0.02	0.09 ± 0.03	0.07 ± 0.03	0.19 ± 0.04	0.36 ± 0.05 ^b	0.31 ± 0.03 ^b	0.31 ± 0.03 ^b	0.11 ± 0.03	0.46 ± 0.11 ^b	0.46 ± 0.11 ^b	0.34 ± 0.03 ^b	0.34 ± 0.03 ^b	0.34 ± 0.03 ^b
Bicarbonate (mmol/L)	26.8 ± 1.6	26.1 ± 0.9	27.9 ± 2.2	26.6 ± 1.5	28.5 ± 2.1	25.9 ± 1.6	26.7 ± 1.1	26.7 ± 1.1	26.5 ± 2.4	26.3 ± 1.8	26.3 ± 1.8	27.3 ± 1.7	27.3 ± 1.7	27.3 ± 1.7

Ctns^{-/-} mice were compared with age-matched wild-type (WT) controls. In addition, 9- and 12-month-old *Ctns*^{-/-} mice were also compared with age-matched CKD mice. Number of mice is ≥8 at each time point. Data are expressed as mean ± SEM. BUN, blood urea nitrogen; TEP, tubular excretion of phosphorus.

^a*p* < 0.05, significantly lower in *Ctns*^{-/-} or CKD mice vs. WT controls.

^b*p* < 0.05, significantly higher in *Ctns*^{-/-} or CKD mice vs. WT controls.

^c*p* < 0.05, significantly different between *Ctns*^{-/-} or CKD mice.

dioxide (VCO_2) consumption were measured. The respiratory exchange ratio (RER) was calculated as the quotient VCO_2/VO_2 . Energy expenditure was measured as a production of kilocalorie of heat and was calculated as Caloric Value (CV) $\times \text{VO}_2$, where CV is $3.815 + 1.232 \times \text{RER}$.¹⁰

Measurement of body composition

Whole body fat mass and lean mass of mice were determined by quantitative magnetic resonance analysis (EchoMRI-100™, Echo Medical Systems).¹¹

Muscle fibre size

Excised soleus and tibialis anterior muscles were snap-frozen in isopentane cooled by liquid nitrogen and stored at -80°C for subsequent analysis. Muscle cross sections (10 μm thick) were taken from muscle midbelly. Sections were first treated with 1% bovine serum albumin and normal goat and mouse serum as blocking agents. Sections were incubated overnight with a polyclonal anti-laminin antibody (Sigma, dilution 1:1000) and then with the secondary antibody, Alexa Fluor 594 goat anti-rabbit immunoglobulin G (Invitrogen, dilution 1:200). The laminin antibody was used to label the fibre perimeter and facilitate fibre area quantification. Sections were imaged with a microscope (Leica CTR 6500, Buffalo Grove) fit with a fluorescent camera (Leica DFC365 FX) set for 594 emission fluorescence using a 10 \times objective. Fibre cross-sectional areas were measured using a custom-written macro in ImageJ (NIH). Filtering criteria were applied to ensure measurement of actual muscle fibres.¹² These criteria rejected regions with areas below 50 μm^2 and above 5000 μm^2 to eliminate neurovascular structures and 'optically fused' fibres, respectively.

Muscle grip strength and rotarod activity

Grip Strength Meter (model 47106, UGO Basile) and AccuRotor Rota Rod (model RRF/SP, Accuscan Instrument) were used to assess forelimb grip strength and motor coordination in mice, respectively.¹³

Uncoupling proteins and pro-inflammatory cytokines

Uncoupling protein (UCP) contents in tissue were assayed using mouse UCP-1 (E95557Mu, Uscn Life Science), UCP-2 (E2066m, EIAab), and UCP-3 (E2068m, EIAab) assay kits, respectively. Sample protein concentration was determined by Pierce BCA protein assay kit. Muscle tissue lysate protein levels of IL-1 α , IL-1 β , IL-6, and TNF- α were quantified with Mouse Quantibody Custom Array (RayBiotech).

Tissue adenosine triphosphate content

Adenosine triphosphate (ATP) concentrations in tissue homogenates were assayed using the ATP colorimetric/fluorometric assay kit (ab83355, Abcam).

Quantitative real-time PCR

RNA was isolated from extracted tissue by using TriZol (Life Technology) and further purified with Direct-zol RNA MiniPre Kit (Zymo Research). cDNA was synthesized using SuperScript III Reverse Transcriptase and oligo(dT)₁₂₋₁₈ primer (Invitrogen). Transcriptional levels of target genes were measured by real-time PCR, using a 7300 Real-Time PCR System (ABI Applied Biosystems). Appropriate primers and probes for target genes were listed (Tables 2 and 3). Comparative $2^{-\Delta\Delta\text{Ct}}$ method was used to determine the relative quantification of target gene. Final results were expressed in arbitrary units, with one unit being the mean mRNA level in the age-matched WT control mice.

Statistical analysis

Results are reported as mean \pm standard error of the mean (SEM). The means of variables were compared with Student's *t*-test, assuming unequal variances, or Welch's analysis of variance, when more than two groups were compared. In that case, a pair-wise *t*-test with Bonferroni correction was performed. The Wilcoxon rank-sum test was used to compare the median of variables. All tests were two-sided. A *P* value of <0.05 was considered significant. Analyses were performed using SPSS 16.0 for Macintosh.

Results

Urine and serum chemistry in *Ctns*^{-/-} mice

We characterized urine and serum chemistry in *Ctns*^{-/-} mice compared with age-matched WT mice at the age of 1, 4, 9, and 12 months. In *Ctns*^{-/-} mice, significantly higher urine phosphate levels and TEP were demonstrated as early as 4 months old relative to controls (Table 1). Proteinuria was evident at 9 months old while polyuria was significant at 12 months old *Ctns*^{-/-} mice. BUN and serum cystatin C levels were significantly higher in *Ctns*^{-/-} mice than controls at 9 months of age. Serum creatinine was significantly higher while creatinine clearance was decreased in *Ctns*^{-/-} mice relative to WT controls at 12 months of age. Serum bicarbonate levels were not different between *Ctns*^{-/-} mice and WT controls.

As *Ctns*^{-/-} mice developed CKD at the age of 9 months, urine and serum chemistry in 9- and 12-month-old *Ctns*^{-/-} mice were compared with age-matched pair-fed CKD mice.

Table 2 PCR primer information

Gene	Forward primer sequence	Reverse primer sequence	Primer bank ID
Acox1	TAATTCCTCACTCGAAGCCA	AGTTCCATGACCCATCTCTGTC	26333821a1
Acs1	TGCCAGAGCTGATTGACATTC	GGCATAACCAGAAGGTGGTGAG	31560705a1
Atg1	AGATGAAAGCAAGATGTTGCCT	CCCTGTAGGTGAGCCATATTCTA	27923915a1
Atrogin-1	CAGCTTCGTGAGCGACCTC	GGCAGTCGAGAAGTCCAGTC	13385848a1
CD137	CGTGCAGAACTCCTGTGATAAC	GTCCACCTATGCTGGAGAAGG	20306992a1
Cidea	TGACATTCATGGGATTGCAGAC	GGCCAGTTGTGATGACTAAGAC	6680944a1
CPT1 α	CTCCGCCTGAGCCATGAAG	CACCAGTGATGATGCCATTCT	27804309a1
CPT1 β	GCACACCAGGCAGTAGCTTT	CAGGAGTTGATTCCAGACAGGTA	6753512a1
Dio2	AATTATGCCTCGGAGAAGACCG	GGCAGTTGCCTAGTGAAAGGT	6753638a1
Gapdh	AGGTCGGTGTGAACGGATTTG	TGTAGACCATGTAGTTGAGGTCA	6679937a1
Glut1	GCCTGACCTTCGGATATGAGC	TGCCATAGCAGTCAATGAGGA	18485498a1
Glut4	GTGACTGGAACACTGGTCCTA	CCAGCCACGTTGCATTGTAG	6678015a1
Hsl	CCAGCCTGAGGGCTTACTG	GTCCATTGACTGTGACATCTCG	26325924a1
IGF-I	CTGGACCAGAGACCTTTGTC	GGACGGGGACTTCTGAGTCTT	6754308a1
MyoD	CCACTCCGGGACATAGACTTG	AAAAGCGCAGGTCTGGTGAG	6996932a1
Myogenin	GAGACATCCCCCTATTCTACCA	GCTCAGTCCGCTCATAGCC	13654247a1
Myostatin	AGTGGAGTAAATGAGGGCAGT	GTTTCAGGCGCAGCTTAC	6754752a1
MuRF-1	GTGTGAGGTGCCTACTTGCTC	GCTCAGTCTTCTGCTTGGA	21523717a1
Pax-3	CCGGGGCAGAATTACCCAC	GCCGTTGATAAATACTCTCCG	26377023a1
Pax-7	TCTCCAAGATTCTGTGCCGAT	CGGGGTTCTCTCTTATACTCC	34328055a1
Pgc1 α	TATGGAGTGACATAGAGTGTGCT	CAGGAGTTGATTCCAGACAGGTA	6679433a1
Pgc1 β	TCCTGTAAAAGCCCGGAGTAT	GCTCTGGTAGGGGCGAGTGA	18875426a1
Ppara α	AGAGCCCCATCTGTCCTCTC	ACTGGTAGTCTGCAAAACCAA	31543500a1
Ppara δ	CAAGTGGGGTCAGTCATGGAA	GCTGGAAGGAAGCGTGTGTT	403943a1
Prdm16	CCCCACATTCGCTGTGAT	CTCGCAATCCTTGCACTCA	124107622c3
Tbx1	CTGTGGGACGAGTTCAATCAG	TTGTATCTACGGGCACAAAG	22094109a1
Tmem26	TTCTGTGTCATTCCCTGGTC	GCCGGAGAAAGCCATTGT	29244332a1

Appropriate primer sequence was obtained from <http://pga.mgh.harvard.edu/primerbank/>

Table 3 Taqman gene expression assays-on-demand identities

Target genes	Assay identities
Cox2	Mm03294838_g1
IL-1 α	Mm00494938_m1
IL-6	Mm00446190_m1
PGF2 α synthase	Mm00442792_m1
TNF- α	Mm00443258_m1
Internal control gene	Assay Identities
Gapdh	4352339E

TEP, volume of 24 h urine excretion, and BUN were elevated while serum creatinine clearance was decreased in 9- and 12-month-old *Ctns*^{-/-} mice than that in CKD mice (Table 1).

Lower body weight, increased energy homeostasis, and muscle wasting in *Ctns*^{-/-} mice

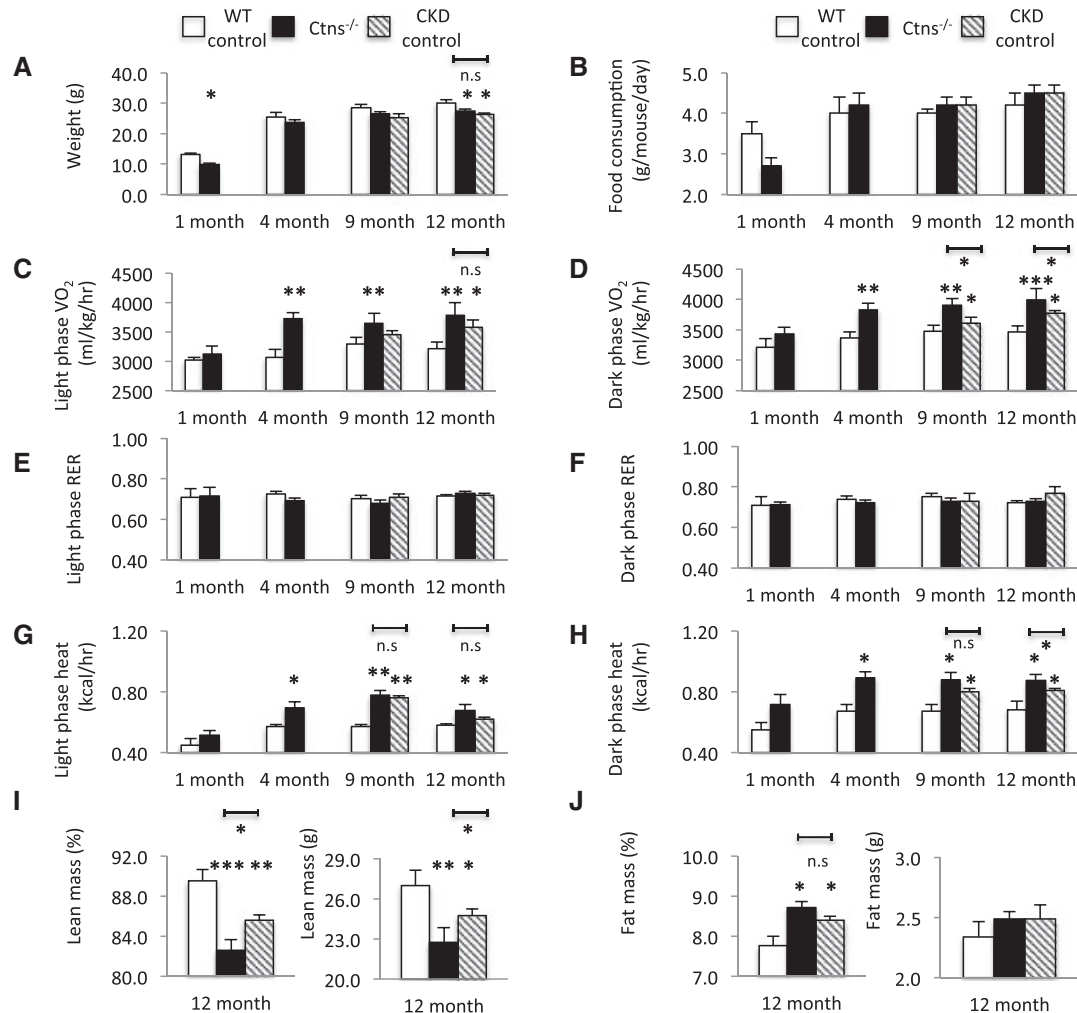
Body mass of *Ctns*^{-/-} mice at 1 month old was 25.8% lighter than age-matched WT controls. At 12 months old, *Ctns*^{-/-} mice were 9.0% lighter than WT controls (Figure 1A). Decreased body weight in *Ctns*^{-/-} mice did not appear to result from reduced food intake. All mice were fed *ad libitum*, and food consumption in *Ctns*^{-/-} mice was not different from WT controls at 1, 4, 9, and 12 months of age (Figure 1B). To further investigate the impact of cystinosis on muscle wasting and energy homeostasis beyond the detrimental effects of

renal dysfunction, age-matched CKD mice were pair-fed to 9- and 12-month-old *Ctns*^{-/-} mice (Figure 1B). Body mass of 9- and 12-month-old *Ctns*^{-/-} mice was comparable with that of pair-fed CKD mice (Figure 1A). *Ctns*^{-/-} mice demonstrated hypermetabolism—their rate of oxygen consumption (VO₂) and heat production in both light and dark phases was significantly higher than that of WT controls as young as 4 months old (Figure 1C, 1D, 1G, and 1H). VO₂ consumption and heat production in dark phase was significantly elevated in 9- and 12-month-old *Ctns*^{-/-} mice than that in pair-fed CKD mice, respectively (Figure 1D and 1H). There was no difference in RER between *Ctns*^{-/-}, WT, and CKD mice (Figure 1E and 1F). At the end of the study, we used quantitative magnetic resonance to analyze body composition. Muscle wasting was evident in *Ctns*^{-/-} and CKD mice vs. WT mice. At 12 months of age, the percentage of lean mass and total lean mass was significantly decreased in *Ctns*^{-/-} than WT or CKD mice (Figure 1I). In contrast, the percentage of fat mass was elevated in *Ctns*^{-/-} mice vs. WT mice while the total fat mass was not different between *Ctns*^{-/-}, WT, and CKD mice (Figure 1J).

Reduced muscle fibre size and impaired muscle function in *Ctns*^{-/-} mice

We studied the effects of cystinosis on skeletal muscle histomorphometry. Muscle sections were labeled for the muscle fibre basement membrane. Representative photomicrographs

Figure 1 Energy homeostasis and body composition in *Ctns*^{-/-} mice. Body mass (A) and food consumption (B); resting metabolic rate (VO₂) of light and dark phase (C and D); light and dark phase respiratory exchange ratio (RER) (E and F); and light and dark phase energy expenditure (G and H). Mice were scanned by quantitative magnetic resonance (QMR) at 12 months of age. Percentage of lean mass, total lean mass, percentage of fat mass, and total fat mass (I and J). Number of mice is ≥8 in each group. Data are expressed as mean ± standard error of the mean. **P* < 0.05, ***P* < 0.01, ****P* < 0.001.



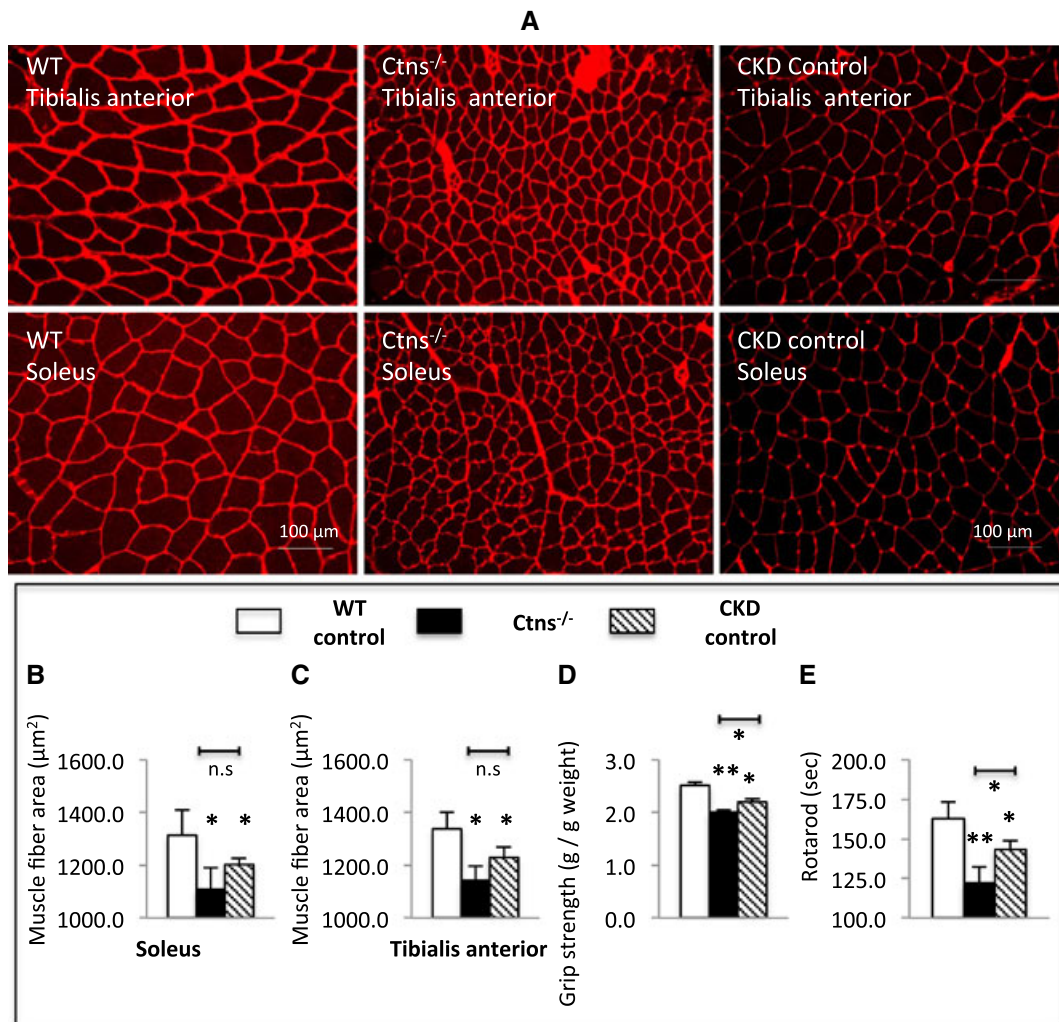
of muscle sections in 12-month-old *Ctns*^{-/-} mice and WT and CKD controls are shown in Figure 2A. Mean soleus and tibialis anterior fibre cross-sectional area in *Ctns*^{-/-} mice was 84.5 and 85.3% of that observed in WT controls (Figure 2B and 2C). Muscle wasting in *Ctns*^{-/-} mice was associated with progressive skeletal muscle weakness. Muscle function, as assessed by forelimb grip strength and rotarod activity, was significantly decreased in *Ctns*^{-/-} mice vs. WT or CKD controls (Figure 2D and 2E).

Muscle wasting signaling in *Ctns*^{-/-} mice

We investigated the signaling pathways associated with skeletal muscle wasting in 12-month-old *Ctns*^{-/-} mice. Gastrocnemius muscle from experimental mice was dissected, and total

RNA from gastrocnemius muscles was extracted and reversely transcribed. Gene expression for several transcripts associated with myogenesis and skeletal regeneration (Pax-3, Pax-7, Myogenin, MyoD, and IGF-I) was significantly decreased in gastrocnemius muscle of *Ctns*^{-/-} mice relative to WT controls (Figure 3A). Gene expression of Pax-3, Pax-7, and Myogenin in *Ctns*^{-/-} mice was significantly lower than that in CKD mice. In contrast, expression of muscle proteolytic genes, Myostatin, Atrogin-1, and MuRF-1, was significantly increased in *Ctns*^{-/-} mice than in WT controls (Figure 3B). In addition, muscle Atrogin-1 and MuRF-1 gene expression in *Ctns*^{-/-} mice was higher than that in CKD controls. Muscle lysate protein levels of inflammatory cytokines (IL-1α, IL-6, and TNF-α) were increased in *Ctns*^{-/-} mice than in WT controls (Figure 3C). Muscle protein content of IL-6 and TNF-α was significantly elevated in *Ctns*^{-/-} mice than in CKD controls.

Figure 2 Skeletal muscle histomorphometry and muscle function in 12-month-old *Ctns*^{-/-} mice. Representative photomicrographs of soleus and tibialis anterior immunohistochemical sections labeled with a polyclonal antibody to laminin with magnification $\times 200$ (A). Soleus muscle and tibialis anterior muscle average fiber area in each group (B) and (C), respectively. Forelimb grip strength (D) and motor coordination (E). Number of mice is ≥ 8 in each group. Data are expressed as mean \pm standard error of the mean. * $P < 0.05$, ** $P < 0.01$.



*Increased thermogenesis and decreased adenosine triphosphate content in skeletal muscle and adipose tissues of *Ctns*^{-/-} mice*

Food consumption of 1- and 4-month-old *Ctns*^{-/-} mice was not different than that of age-matched WT controls (Figure 1B). The observed lower body mass in young *Ctns*^{-/-} mice may be associated with disturbances in energy homeostasis before the onset of renal dysfunction. We measured muscle and liver ATP content in 1- and 4-month-old *Ctns*^{-/-} mice vs. WT controls. Gastrocnemius muscle ATP was significantly decreased in *Ctns*^{-/-} mice relative to age-matched WT controls (Figure 4A and 4C).

Protein contents of UCPs in gastrocnemius muscle and adipose tissues were elevated in 12-month-old *Ctns*^{-/-} mice

relative to WT (Figure 5A, 5C, 5E, and 5G). Protein contents of UCP-1 and UCP-2 in adipose tissue were increased in 12-month-old *Ctns*^{-/-} mice vs. age-matched CKD mice. In contrast, ATP contents in muscle and inguinal white adipose tissue (WAT) were markedly decreased in *Ctns*^{-/-} mice relative to WT and CKD controls (Figure 5B and 5H). ATP contents in interscapular brown adipose tissue (BAT) and epididymal WAT were decreased in *Ctns*^{-/-} mice than in WT control but were not different than those in age-matched CKD controls (Figure 5D and 5F).

We compared expression profile of genes related to energy consumption in 12-month-old *Ctns*^{-/-} mice. The expression levels of genes related to fatty acid oxidation (*Ppar α* , *Ppar δ* , and *Cpt1 α*) and energy consumption (*Pgc1 α* and *Pgc1 β*) were increased in the skeletal muscle of *Ctns*^{-/-} mice than in that of WT controls (Figure 6A). In addition, *Pgc1 α* and *Pgc1 β* gene

Figure 3 Gene expression of key molecules implicated in muscle wasting in 12-month-old *Ctns*^{-/-} mice (A and B) and muscle pro-inflammatory cytokine protein contents (C). Comparative 2- $\Delta\Delta$ Ct method was used to determine the relative quantification of genes in muscle. To normalize each sample for RNA content, the internal control gene GAPDH was used. Final results were expressed in arbitrary units, with one unit being the mean mRNA level in the wild-type controls. Data are expressed as mean \pm standard error of the mean. * $P < 0.05$, ** $P < 0.01$, *** $P < 0.001$.

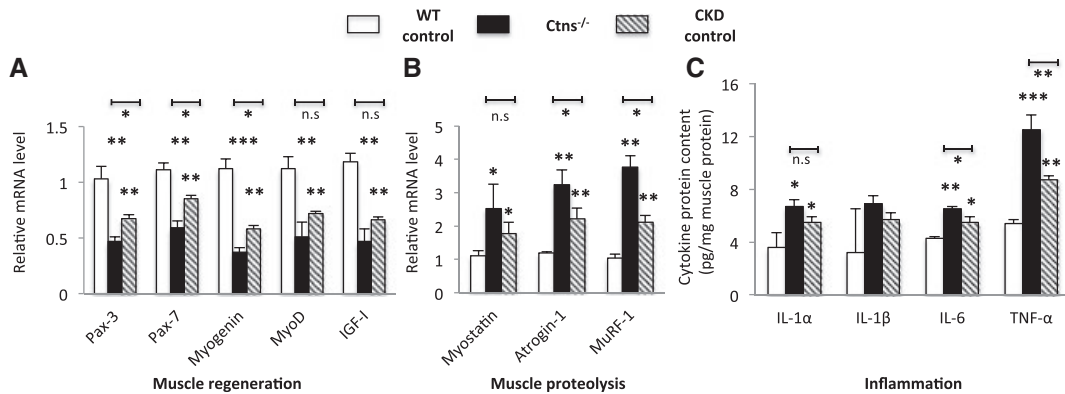
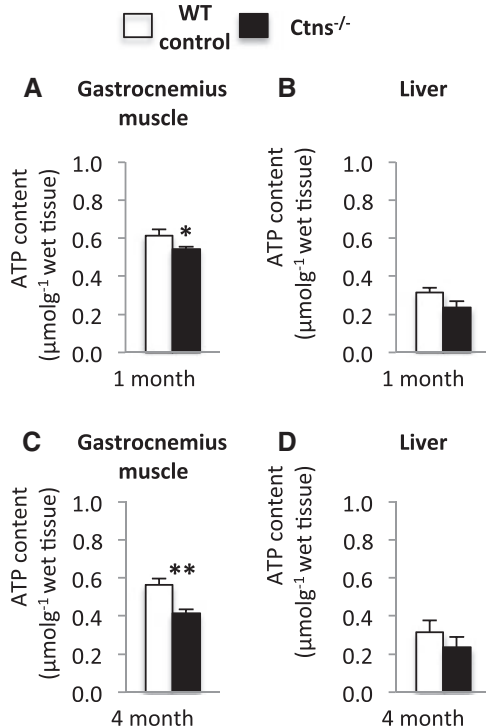


Figure 4 Adenosine triphosphate content in muscle and liver in 1- and 4-month-old *Ctns*^{-/-} mice. Adenosine triphosphate content in tissue lysate was measured in duplicate and calculated per gram of tissue. Number of mice is ≥ 6 in each group. Data are expressed as mean \pm standard error of the mean. * $P < 0.05$, ** $P < 0.01$, *** $P < 0.001$.



expression in *Ctns*^{-/-} mice was significantly higher than that in CKD mice. Increased thermogenic gene expression (Ppargc1 α , Pgc1 α , Cidea, Prdm16, and Dio2) was found in BAT of *Ctns*^{-/-} mice than in WT controls (Figure 6B).

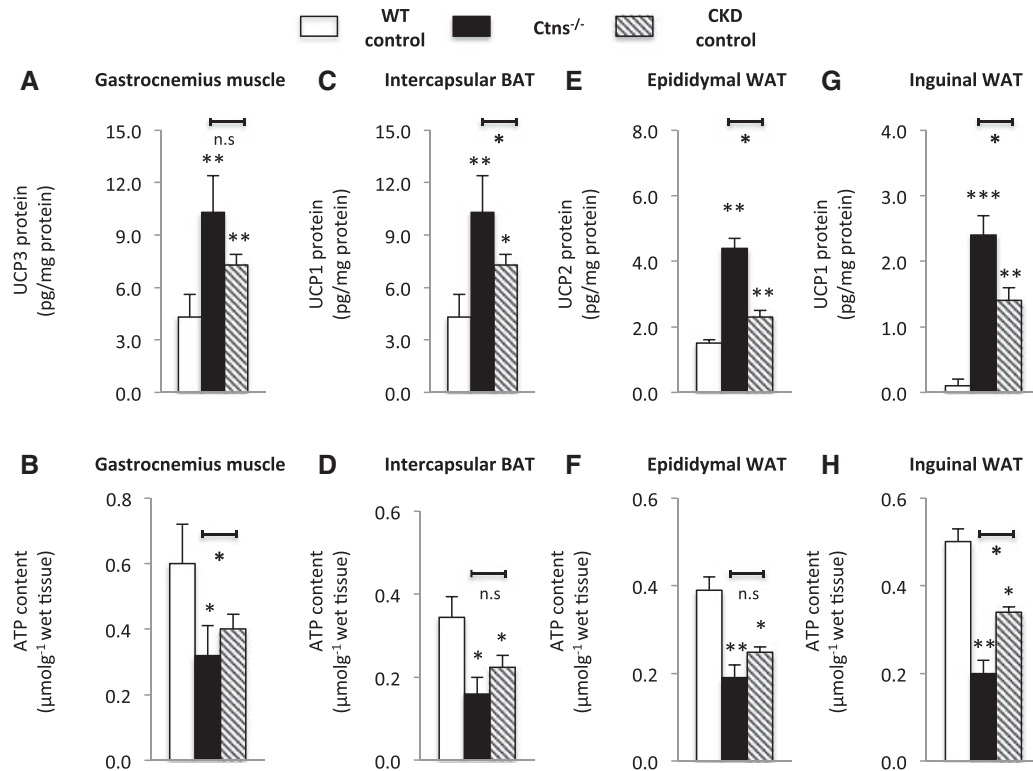
Epididymal WAT exhibited higher expression of Ppargc1 α , Pgc1 α , and glucose transporter Glut1 in *Ctns*^{-/-} mice than in WT controls, but no difference was found in expression of genes involved in lipolytic metabolism (Acox1, Acsl1, Atg1, and Hsl) in *Ctns*^{-/-} mice relative to WT or CKD mice (Figure 6C). Moreover, inguinal WAT of *Ctns*^{-/-} mice displaced higher expression of Ppargc1 α , Pgc1 α , Cidea, Prdm16, and Dio2 than that of WT controls (Figure 6D).

Adipose tissue browning in *Ctns*^{-/-} mice

Beige adipocytes are a distinct type of thermogenic fat cells in mice and humans. Browning of beige adipocytes in WAT has been associated with increased energy expenditure in cachexia. We observed elevated expression of beige adipose cell surface markers (CD137, Tmem26, and Tbx1) in inguinal WAT in 12-month-old *Ctns*^{-/-} mice than in WT controls (Figure 7A). Furthermore, inguinal WAT CD137 and Tbx1 expression was higher in *Ctns*^{-/-} mice than in CKD controls. Another important marker for beige adipocyte in inguinal WAT is UCP-1, which is usually not detected in WAT. UCP-1 protein was detected in inguinal WAT of 12-month-old *Ctns*^{-/-} and CKD mice but was undetectable in WT controls (Figure 5G). UCP-1 protein level in inguinal WAT of 12-month-old *Ctns*^{-/-} was higher than that in CKD mice. Collectively, these results demonstrate the development of beige adipocytes in 12-month-old *Ctns*^{-/-} mice. Our results show that increased energy expenditure is associated with adipose tissue browning in *Ctns*^{-/-} mice.

We also measured gene expression of key molecules implicated in the pathogenesis of WAT browning in mice. Inguinal WAT of 12-month-old *Ctns*^{-/-} mice displayed higher mRNA expression of Cox2 and PGF2 α than that of WT controls (Figure 7B). Gene expression of inflammatory cytokines, IL-1 α , IL-6, and TNF- α , was significantly elevated in inguinal

Figure 5 Uncoupling protein level and adenosine triphosphate content in muscle and adipose tissue of 12-month-old *Ctns*^{-/-} mice. Uncoupling protein content (A, C, E, and G) and adenosine triphosphate content (B, D, F, and H) in tissue were measured. Number of mice is ≥ 6 in each group. Data are expressed as mean \pm standard error of the mean. * $P < 0.05$, ** $P < 0.01$.



WAT of 12-month-old *Ctns*^{-/-} mice than that in age-matched WT controls or CKD mice (Figure 7B).

Discussion

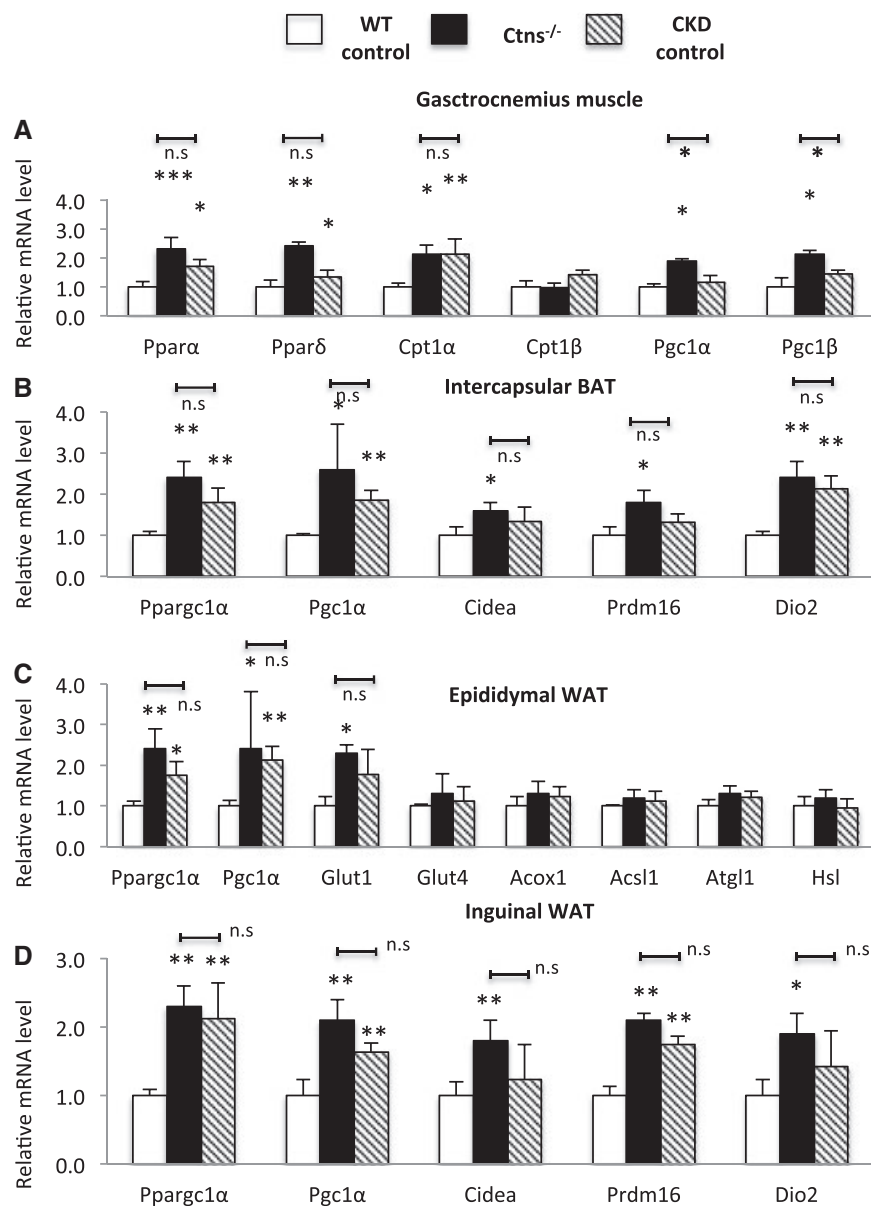
This study confirms the presence of the tubular and glomerular dysfunction in *Ctns*^{-/-} mice. Fanconi syndrome, the hallmark of the tubular dysfunction in children with INC, characterized by phosphaturia, proteinuria, and polyuria, was demonstrated in *Ctns*^{-/-} mice (Table 1). Indeed, elevation of TEP index, the more sensitive parameter of tubular function, was demonstrated earlier in the course of the renal disease (4 months of age) than the glomerular dysfunction (9 months of age). Serum cystatin C is a reliable marker for renal function in mice and humans, which has the advantage over serum creatinine when muscle wasting can be a confounding factor.^{14,15} Serum cystatin C levels were elevated in *Ctns*^{-/-} mice than in controls at 9 months of age. The time course of renal dysfunction in *Ctns*^{-/-} mice of this study is in concordance with a recent report.¹⁶

Importantly, we show that *Ctns*^{-/-} mice exhibit disturbances in energy homeostasis prior to the development of

CKD. Basal metabolic rate comprises 50–80% of daily energy expenditure and exhibits circadian rhythms. Food consumption in *Ctns*^{-/-} mice was not different than age-matched WT controls (Figure 1B). However, significantly lower total body mass starting at 1 month of age as well as increased energy expenditure at 4 months of age (Figure 1A, 1C, 1D, 1G, and 1H) preceded the onset of CKD at 9 months of age in *Ctns*^{-/-} mice (Table 1). Muscle ATP content in 1- and 4-month-old *Ctns*^{-/-} mice was significantly lower than that in age-matched WT controls (Figure 4A and 4C). We compared parameters of energy homeostasis in 9- and 12-month-old *Ctns*^{-/-} mice vs. pair-fed age-matched CKD mice. VO_2 and energy expenditure at dark phase was significantly elevated in 9- and 12-month-old *Ctns*^{-/-} mice than that in CKD controls (Figure 1D and 1H).

Muscle wasting is a life-threatening complication in cystinosis.^{2,6} We observed decreased body mass and lean mass in 12-month-old *Ctns*^{-/-} mice than in WT control or pair-fed CKD mice (Figure 1A and 1I). We further measured muscle fibre histomorphometry and muscle function in *Ctns*^{-/-} mice. Soleus and tibialis anterior muscle were chosen as they represent extremes of mouse muscle types in terms of fibre type composition¹⁷ since the soleus is composed of about 50% type 1 fibre (slow) while the tibialis anterior has

Figure 6 Thermogenic gene expression in 12-month-old *Ctns*^{-/-} mice. Thermogenic gene expression in skeletal muscle and adipose tissues (A to D). Number of mice = 6. Data are expressed as mean \pm standard error of the mean. * $P < 0.05$, ** $P < 0.01$, *** $P < 0.001$.



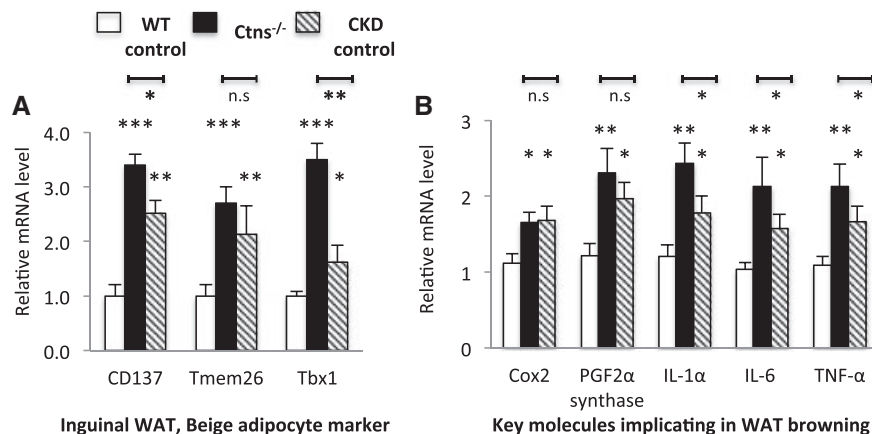
no slow fibres. Cross-sectional area of soleus and tibialis anterior was significantly reduced in *Ctns*^{-/-} mice than in WT controls (Figure 2A, 2B, and 2C). We also showed that reduced muscle mass and decreased muscle fibre cross-sectional area correlate with reduced grip strength and impaired rotarod activity in *Ctns*^{-/-} mice than in WT and CKD mice (Figure 2D and 2E). Reduced cross-sectional area of muscle is not always associated with diminished muscle strength in cachectic patients.^{18,19}

Our results suggest that loss of lean mass, decreased muscle fibre cross-sectional area, and impaired muscle function are more severe in 12-month-old *Ctns*^{-/-} mice than in

age-matched pair-fed CKD controls. Indeed, muscle wasting in children with nephropathic cystinosis seems to be more prevalent than in CKD children with comparable degree of renal dysfunction. Although there is no direct comparison, muscle wasting is highly prevalent in patients with nephropathic cystinosis with predialysis CKD (33–60% in two long-term follow-up studies).^{4,5} On the other hand, a recent study showed no appendicular lean mass deficits in children with mild to moderate CKD.²⁰

We studied muscle mass regulatory signaling pathways in *Ctns*^{-/-} mice. mRNA contents of Pax-3 and Pax-7, Myogenin, and MyoD were decreased in the gastrocnemius muscle of

Figure 7 Adipose tissue browning in 12-month-old *Ctns*^{-/-} mice. Gene expression of beige adipocyte marker (CD137, Tmem26, and Tbx1) in inguinal white adipose tissue was measured (A). Gene expression of key molecules implicated in adipose tissue browning (B). Results were analysed and expressed as in Figure 3. **P* < 0.05, ***P* < 0.01, ****P* < 0.001.



12-month-old *Ctns*^{-/-} mice (Figure 3A), suggesting altered satellite cell content or activity and reduced myoblast differentiation in *Ctns*^{-/-} mice. Expression of muscle IGF-I was down-regulated while Myostatin mRNA was up-regulated in *Ctns*^{-/-} mice (Figure 3A and 3B). IGF-I and Myostatin play stimulatory and inhibitory roles, respectively, in the regulation of muscle mass.²¹ Expression of muscle atrophy-associated genes, Atrogin-1 and MuRF-1, was significantly increased in *Ctns*^{-/-} mice relative to WT controls (Figure 3B). Muscle protein contents of IL-1α, IL-6, and TNF-α were significantly increased in *Ctns*^{-/-} mice than in WT controls (Figure 3C). Inflammatory cytokines have been implicated in the pathogenesis of muscle wasting.^{22,23}

Skeletal muscle accounts for 20–30% of overall energy consumption at rest.^{24,25} Chronic inflammation in skeletal muscle may cause hypermetabolism in *Ctns*^{-/-} mice. We showed that muscle inflammatory cytokines (IL-1α, IL-6, and TNF-α) were significantly increased in *Ctns*^{-/-} mice (Figure 3C). Common causes of chronic inflammation include deterioration of renal function, volume overload, alternation in body composition, and acidosis.^{22,23} Metabolic acidosis is unlikely the culprit in *Ctns*^{-/-} mice as they were not acidotic. Serum bicarbonate level in *Ctns*^{-/-} mice was not different from that in controls (Table 1).

Recent studies suggest that UCP-1 contributes to adaptive thermogenesis while UCP-2 and UCP-3 are involved in the resting metabolic rate.²⁶ We investigated the mechanisms of hypermetabolism in *Ctns*^{-/-} mice. Protein contents of UCP-2 and UCP-3 were increased in muscle and WAT of *Ctns*^{-/-} mice than in WT controls (Figure 5A and 5E). In contrast, ATP contents in muscle and adipose tissue were decreased in *Ctns*^{-/-} mice relative to controls (Figure 5B and 5F). In addition, increased UCP-1 and decreased ATP contents in adipose tissue were observed in *Ctns*^{-/-} mice than in WT controls (Figure 5C, 5D, 5G, and 5H). Adipose tissue is also

important in energy metabolism. We, and others, have previously described the increased thermogenesis and up-regulation of UCPs in adipose tissue in rodent models of cachexia and in cachectic patients.^{9,13,27–31} Up-regulation of UCPs expression promotes proton leak and reduces cellular ATP production in exchange for the generation of heat.^{32,33} *In vitro* studies have reported that modest increase in the expression of UCP-2 leads to rapid fall in mitochondrial membrane potential and a reduction of intracellular ATP content.³⁴ UCP-3 modulates the activity of sacro/endoplasmic reticulum Ca²⁺-ATPase and decreases mitochondrial ATP production.³⁵ Several studies have reported decreased levels of ATP in cystinotic cells, including fibroblast, leucocytes, and renal epithelial cells.³⁶ Abnormal ATP production has been associated with impaired respiratory chain complex I activity in cystinotic cells.³⁷

We also profiled expression of genes related to energy consumption in skeletal muscles of *Ctns*^{-/-} mice. PPARα and PPARδ as well as CPT1α and CPT1β are key regulators of fatty acid oxidation in muscle.^{38,39} Transcriptional levels of PPARα, PPARδ, and CPT1α were significantly up-regulated in the skeletal muscle of *Ctns*^{-/-} mice (Figure 6A). This profile has been associated with increased resting metabolic rate and maintenance of leanness in humans.⁴⁰ Activated fatty acid oxidation is associated with up-regulation of PGC1α and PGC1β, two key molecules involved in the regulation of mitochondrial energy metabolism.^{41,42} This was also confirmed in *Ctns*^{-/-} mice (Figure 6A). In addition, we demonstrated increased expression of thermogenic genes in BAT, and epididymal and inguinal WAT of *Ctns*^{-/-} mice (Figure 6B, 6C, and 6D). UCP-2 and UCP-3 regulate fatty acid metabolism in skeletal muscle and adipose cells. UCP-2 and UCP-3 promote fatty acid metabolism by exporting fatty acid anions outside of the mitochondrial matrix.²⁶ Collectively, our results suggest that up-regulation of UCPs, elevated key molecules of fatty acid oxidation, and mitochondrial energy metabolism in

muscle and adipose tissue may be implicated in the pathogenesis of hypermetabolism in $Ctns^{-/-}$ mice.

Adipose tissue browning has recently been reported in cancer cachexia.³¹ White fat depots contain pockets of UCP-1-expressing multiocular cells, called beige (or brite) cells, that can be stimulated on exposure to cold or other stimuli via the process termed browning.⁴³⁻⁴⁵ Epididymal WAT predominantly contains white adipocytes while inguinal WAT contains a mixed population of white and beige adipocytes.⁴⁶ We demonstrated increased expression of unique beige adipose cell markers (CD137, Tmem26, and Tbx1) and BAT marker UCP1 in inguinal WAT of $Ctns^{-/-}$ mice (Figures 5G and 7A). Our results suggest the development of beige adipocytes in $Ctns^{-/-}$ mice. The development of browning and beige adipocytes in $Ctns^{-/-}$ mice is a novel finding. The mechanism is currently unknown. Recent evidence shows that transdifferentiation of white adipocytes and *de novo* differentiation of beige adipocyte coexist.⁴⁶ Beige adipocyte precursors have also been identified in skeletal muscle,⁴⁷ which further underlies the complexity of beige adipogenesis. Transcriptional regulator PPAR γ is necessary and sufficient for adipogenesis. The actions of PPAR γ are modulated by a large set of proadipogenic transcriptional cofactors.⁴⁶ We demonstrated increased expression of PPARGC1 α , CIDEA, PDRM16, and DIO2 in inguinal WAT of $Ctns^{-/-}$ mice (Figure 6D). The important roles of transcriptional factors DIO2, PDRM16, PPARGC1 α , and CIDEA on adipogenesis and thermogenesis have been described.^{46,48} Overexpression of these transcriptional cofactors in WAT favors adipocyte browning and thermogenesis.

WAT browning is responsible for a significant increase in total energy expenditure.⁴⁹ Several mechanisms have been proposed for WAT browning, including activation of Cox2 signaling pathway and chronic inflammation. Activation of Cox2, a downstream effector of β -adrenergic signaling, is crucial for the induction of brown fat-like cells in WAT depots.⁵⁰ Cox2 produces prostaglandins that enhance mitochondrial biogenesis and increase the uncoupling capacity when activated with adrenergics.⁵¹ We showed that inguinal WAT gene expression of Cox2 and PGF2 α was significantly increased in $Ctns^{-/-}$ mice vs. WT control mice (Figure 7B). Chronic inflammation is a hallmark of both clinical and experimental cachexia.^{22,23,52,53} Inflammatory cytokines, such as IL-6, play an important role in the WAT browning phenotype in mouse models of cachexia.⁵⁴ Gene expression of IL-1 α , IL-6, and TNF- α was significantly elevated in inguinal WAT of 12-month-old $Ctns^{-/-}$ mice than that in age-matched WT controls or CKD mice (Figure 7B). Inflammation in WAT is characterized by recruitment of macrophages, including activated M1 and M2 macrophages.⁵⁵ Activated macrophages in the WAT are an important source of adrenaline and noradrenaline and have been associated with an increase in uncoupled respiration and energy expenditure in mice.⁵⁶ We showed that the phenomenon of adipose tissue browning was more advanced in 12-month-old $Ctns^{-/-}$ vs. CKD controls, as indicated by the

higher expression of browning markers CD137 and Tbx1 (Figure 7A). At the same time, there was evidence of more severe inflammation in the $Ctns^{-/-}$ mice compared with CKD controls as indicated by the inflammatory cytokine expression levels of IL-1 α , IL-6, and TNF- α in inguinal WAT (Figure 7B). We postulate that inflammation is an important mechanism underlying the adipose tissue browning in INC.

Conclusion

We describe muscle wasting and adipose tissue browning in a mouse model of INC. We show that $Ctns^{-/-}$ mice exhibit disturbances in energy homeostasis before the onset of their CKD. We demonstrate aberrant muscle mass regulatory signaling pathways in $Ctns^{-/-}$ mice. We show that hypermetabolism in $Ctns^{-/-}$ mice is associated with up-regulation of key enzymes regulating thermogenesis in skeletal muscle and adipose tissues. Importantly, we report novel findings in the development of beige adipocytes in $Ctns^{-/-}$ mice. Further studies are required to investigate the underlying mechanisms of these metabolic defects in INC, which are associated with poor quality of life and mortality, and for which there is no current therapy.

Acknowledgements

The authors certify that they comply with the ethical guidelines for authorship and publishing of the *Journal of Cachexia, Sarcopenia and Muscle* (von Haehling S, Morley JE, Coats AJS, Anker SD. Ethical guidelines for authorship and publishing in the *Journal of Cachexia, Sarcopenia and Muscle*. *J Cachexia Sarcopenia Muscle*. 2010;1:7–8.)

We gratefully acknowledge Professor Corinne Antignac for providing the $Ctns^{-/-}$ mice. This work is supported in part by funding from Cystinosis Research Foundation. R.H.M. received funding from National Institutes of Health (NIH) U01DK03012; S.C. received funding from NIH Grant RO1-DK090058 and RO1-DK099338. P.Z. was supported by Education Department of Heilongjiang province (no. 12541324), Harbin Science & Technology Bureau (no. 2014RFXJ077), and China Scholarship Council (no. 201308230141). R.L.L. received funding from NIH Grant R24-HD050837. This work was supported by NIH Grant R24-HD050837 to create the National Skeletal Muscle Research Center (NSMRC) at University of California, San Diego.

Conflict of interest

The authors declare they have no conflicts of interest.

References

1. Town M, Jean G, Cherqui S, Attard M, Forestier L, Whitmore SA, et al. A novel gene encoding an integral membrane protein is mutated in nephropathic cystinosis. *Nat Genet* 1998; **18**: 319–324.
2. Gahl WA, Thoene JG, Schneider JA. Cystinosis. *N Engl J Med* 2002; **347**: 111–121.
3. Nesterova G, Gahl W. Nephropathic cystinosis: late complications of a multisystemic disease. *Pediatr Nephrol* 2008; **23**: 863–878.
4. Gahl WA, Balog JZ, Kleta R. Nephropathic cystinosis in adults: natural history and effects of oral cysteamine therapy. *Ann Intern Med* 2007; **147**: 242–250.
5. Brodin-Sartorius A, Tete M-J, Niaudet P, Antignac C, Guest G, Ottolenghi C, et al. Cysteamine therapy delays the progression of nephropathic cystinosis in late adolescents and adults. *Kidney Int* 2012; **81**: 179–189.
6. Theodoropoulos DS, Krasnewich D, Kaiser-Kupfer MI, Gahl WA. Classic nephropathic cystinosis as an adult disease. *JAMA* 1993; **270**: 2200–2204.
7. Wilmer MJ, Emma F, Levchenko EN. The pathogenesis of cystinosis: mechanisms beyond cysteine accumulation. *Am J Physiol Renal Physiol* 2010; **299**: F905–F916.
8. Kalatzis V, Antignac C. New aspects of the pathogenesis of cystinosis. *Pediatr Nephrol* 2003; **18**: 207–215.
9. Cheung WW, Kuo HJ, Markison S, Chen C, Foster AC, Marks DL, et al. Peripheral administration of the melanocortin-4 receptor antagonist NBI-12i ameliorates uremia-associated cachexia in mice. *J Am Soc Nephrol* 2007; **18**: 2517–2524.
10. Ferrannini E. The theoretical bases of indirect calorimetry: a review. *Metabolism* 1988; **37**: 287–301.
11. Cheung WW, Mak RH. Melanocortin antagonism ameliorates muscle wasting and inflammation in chronic kidney disease. *Am J Physiol Renal Physiol* 2012; **303**: F1315–F1324.
12. Weibel ER. Practical methods for biological morphometry. In *Stereological Methods*. New York, NY: Academic Press; 1980.
13. Cheung WW, Ding W, Gunta SS, Gu Y, Tabakman R, Klapper LN, et al. A pegylated leptin antagonist ameliorates CKD-associated cachexia in mice. *J Am Soc Nephrol* 2014; **25**: 119–128.
14. Song S, Meyer M, Türk TR, Wilde B, Feldkamp T, Assert R, et al. Serum cystatin C in mouse model: a reliable and precise marker for renal function and superior to serum creatinine. *Nephrol Dial Transplant* 2009; **24**: 1157–1161.
15. Shlipak MG, Matsushita K, Ärnlöv J, Inker LA, Katz R, Polkinghorne KR, et al. Cystatin C versus creatinine in determining risk based on kidney function. *N Engl J Med* 2013; **369**: 932–943.
16. Gaide Chevonnay HP, Janssens V, Van Der Smissen P, N'kuli F, Nevo N, Guiot Y, et al. Time course of pathogenic and adaptation mechanisms in cystinotic mouse kidneys. *J Am Soc Nephrol* 2014; **25**: 1256–1269.
17. Burkholder TJ, Fingado B, Baron S, Lieber RL. Relationship between muscle fiber types and sizes and muscle architectural properties in the mouse hindlimb. *J Morphol* 1994; **221**: 177–190.
18. Christensen JF, Andersen JL, Adamsen L, Lindegaard B, Mackey AL, Nielsen RH, et al. Progressive resistance training and cancer testis (PROTRACT)—efficacy of resistance training on muscle function, morphology and inflammatory profile in testicular cancer patients undergoing chemotherapy: design of a randomized controlled trial. *BMC Cancer* 2011; **11**: 326.
19. Hilaire G, Voituren N, Menuet C, Ichiyama RM, Subramanian HH, Dutschmann M. The role of serotonin in respiratory function and dysfunction. *Respir Physiol Neurobiol* 2010; **174**: 76–88.
20. Foster BJ, Kalkwarf HJ, Shults J, Zemel BS, Wetzsteon RJ, Thayu M, et al. Association of chronic kidney disease with muscle deficits in children. *J Am Soc Nephrol* 2011; **22**: 377–386.
21. Mak RH, Rotwein P. Myostatin and insulin-like growth factors in uremic sarcopenia: the yin and yang in muscle mass regulation. *Kidney Int* 2006; **70**: 410–412.
22. Mak RH, Cheung WW, Zhan JY, Shen Q, Foster BJ. Cachexia and protein-energy wasting in children with chronic kidney disease. *Pediatr Nephrol* 2012; **27**: 173–181.
23. Mak RH, Ikizler AT, Kovesdy CP, Raj DS, Stenvinkel P, Kalantar-Zadeh K. Wasting in chronic kidney disease. *J Cachexia Sarcopenia Muscle* 2011; **2**: 9–25.
24. van den Berg SA, van Marken Lichtenbelt W, Willems van Dijk K, Schrauwen P. Skeletal muscle mitochondrial uncoupling, adaptive thermogenesis and energy expenditure. *Curr Opin Clin Nutr Metab Care* 2011; **14**: 243–249.
25. Zurlo F, Larson K, Bogardus C, Ravussin E. Skeletal muscle metabolism is a major determinant of resting energy expenditure. *J Clin Invest* 1990; **86**: 1423–1427.
26. Rousset S, Alves-Guerra MC, Mozo J, Miroux B, Cassard-Doulcier AM, Bouillaud F, et al. The biology of mitochondrial uncoupling proteins. *Diabetes* 2004; **53**: S130–S135.
27. Bing C, Brown M, King P, Collins P, Tisdale MJ, Williams G. Increased gene expression of brown fat uncoupling protein (UCP) and skeletal UCP2 and UCP3 in MAC-16 induced cancer cachexia. *Cancer Res* 2000; **60**: 2405–2410.
28. Tsoli M, Moore M, Burg D, Painter A, Taylor R, Lockie SH, et al. Activation of thermogenesis in brown adipose tissue and dysregulated lipid metabolism associated with cancer cachexia in mice. *Cancer Res* 2012; **72**: 4372–4382.
29. Bianchi A, Bruce J, Cooper AL, Childs C, Kohli M, Morris ID, et al. Increased brown adipose tissue activity in children with malignant disease. *Horm Metab Res* 1989; **21**: 640–641.
30. Shellock FG, Riedinger MS, Fishbein MC. Brown adipose tissue in cancer patients: possible cause of cancer-induced cachexia. *J Cancer Res Clin Oncol* 1986; **111**: 82–85.
31. Kir S, White J, Kleiner S, Kazak L, Cohen P, Baracos VE, et al. Tumour-derived PTH-related protein triggers adipose tissue browning and cancer cachexia. *Nature* 2014; **513**: 100–104.
32. Argiles JM, Busquets S, Lopez-Soriano FJ. The role of uncoupling proteins in pathophysiological states. *Biochem Biophys Res Commun* 2002; **293**: 1145–1152.
33. Sluse FE. Uncoupling proteins: molecular, functional, regulatory, physiological and pathological aspects. *Adv Exp Med Biol* 2012; **942**: 137–156.
34. Mills EM, Xu D, Fergusson MM, Comb CA, Xu Y, Finkel T. Regulation of cellular oncosis by uncoupling protein 2. *J Biol Chem* 2002; **277**: 27385–27392.
35. De Marchi U, Castelbou C, Demareux N. Uncoupling protein 3 (UCP3) modulates the activity of sarco/endoplasmic reticulum Ca²⁺ -ATPase (SERCA) by decreasing mitochondrial ATP production. *J Biol Chem* 2012; **286**: 32533–32541.
36. Levchenko EN, Wilmer MJ, Janseen AJ, Koenderink JB, Visch HJ, Willems PH, et al. Decreased intracellular ATP content and intact mitochondrial energy generating capacity in human cystinosis fibroblasts. *Pediatr Res* 2006; **59**: 287–292.
37. Sansanwal P, Yen B, Gahl WA, Ma Y, Ying L, Wong LJ, et al. Mitochondrial autophagy promotes cellular injury in nephropathic cystinosis. *J Am Soc Nephrol* 2010; **21**: 272–283.
38. Barish GD, Narkar VA, Evans RM. PPAR delta: a dagger in the heart of the metabolic syndrome. *J Clin Invest* 2006; **116**: 590–597.
39. Wakil SJ, Abu-Elheiga LA. Fatty acid metabolism: target for metabolic syndrome. *J Lipid Res* 2009; **50**: S138–S143.
40. Stephens FB, Wall BT, Marimuthu K, Shannon CE, Constantin-Teodosiu D, Macdonald IA, et al. Skeletal muscle carnitine loading increases energy expenditure, modulates fuel metabolism gene networks and prevents body fat accumulation in humans. *J Physiol* 2013; **591**: 4655–4666.
41. Mandart S, Müller M, Kersten S. Peroxisome proliferator-activated receptor α target genes. *Cell Mol Life Sci* 2004; **61**: 393–416.
42. Austin S, St-Pierre J. PGC1 α and PGC1 β , two key molecules involved in the regulation of mitochondrial energy metabolism. *J Cell Sci* 2012; **125**: 4963–4971.
43. Cypess AM, Lehman S, Williams G, Tal I, Rodman D, Goldfine AB, et al. Identification and importance of brown adipose tissue in adult humans. *N Engl J Med* 2009; **360**: 1509–1517.
44. Van Marken Lichtenbelt WD, Smulders NM, Drossaerts JM, Kemerink GJ, Bouvy ND,

- Schrauwen P, *et al.* Cold-activated brown adipose tissue in healthy men. *N Engl J Med* 2009; **360**: 1500–1508.
45. Wu J, Bostrom P, Sparks LM, Ye L, Choi JH, Giang AH, *et al.* Beige adipocytes are a distinct type of thermogenic fat cell in mouse and human. *Cell* 2012; **150**: 366–376.
 46. Bartelt A, Heeren J. Adipose tissue browning and metabolic health. *Nat Rev Endocrinol* 2014; **10**: 24–36.
 47. Schulz T, Huang TL, Tran TT, Zhang H, Townsend KL, Shadrach JL, *et al.* Identification of inducible adipocyte progenitors residing in skeletal muscle and white fat. *Proc Natl Acad Sci U S A* 2011; **108**: 143–148.
 48. Lo KA, Sun L. Turning WAT into BAT: a review on regulators controlling the browning of white adipocytes. *Biosci Rep* 2013; **33**: e00065.
 49. Shabalina IG, Petrovic N, de Jong JM, Kalinovich AV, Cannon B, Nedergaard J. UCP1 in brite/beige adipose tissue mitochondria is functionally thermogenic. *Cell Rep* 2013; **5**: 1196–1203.
 50. Vegiopoulos A, Muller-Decker K, Strzoda D, Schmitt I, Chichelnitskiy E, Ostertag A, *et al.* Cyclooxygenase-2 controls energy homeostasis in mice by de novo recruitment of brown adipocytes. *Science* 2010; **328**: 1158–1161.
 51. Barbatelli G, Murano L, Madsen Q, Han M, Jimenez K, Kristiansen JP, *et al.* The emergence of cold-induced brown adipocytes in mouse white fat depots is determined predominantly by white to brown adipocyte transdifferentiation. *Am J Physiol Endocrinol Metab* 2010; **298**: E1244–E1253.
 52. Blum D, Omlin A, Baracos VE, Solheim TS, Tan BH, Stone P, *et al.* European palliative care research collaborative. Cancer cachexia: a systematic literature review of items and domains associated with involuntary weight loss in cancer. *Crit Rev Oncol Hematol* 2011; **80**: 114–144.
 53. Fearon K, Glass DJ, Guttridge DC. Cancer cachexia: mediators, signaling, and metabolic pathways. *Cell Metab* 2012; **16**: 153–166.
 54. Petruzzelli M, Schweiger M, Schreiber R, Campos-Olivas R, Tsoli M, Allen J, *et al.* A switch from white to brown fat increases energy expenditure in cancer-associated cachexia. *Cell Metab* 2014; **20**: 433–447.
 55. Shen W, Chuang CC, Martinez K, Reid T, Brown JM, Xi L, *et al.* Conjugated linoleic acid reduces adiposity and increases markers of browning and inflammation in white adipose tissue of mice. *J Lipid Res* 2013; **54**: 909–922.
 56. Nguyen KD, Qiu Y, Cui X, Goh YPS, Mwangi J, David T, *et al.* Alternatively activated macrophages produce catecholamines to sustain adaptive thermogenesis. *Nature* 2011; **480**: 104–108.